frontiers | Frontiers in Earth Science

ORIGINAL RESEARCH
published: 06 April 2022
doi: 10.3389/feart.2022.840667

Microscopic Characteristics of Fault Gouge in Minor-Surface-Rupture Faults: A Case Study in the Longmenshan Fault Zone, Eastern Tibetan

Yanbao Li[1], *Lichun Chen*[1,2]*, *Yongkang Ran*[1] *and Yuqiao Chang*[3]

[1]Institute of Geology, China Earthquake Administration, Beijing, China, [2]College of Earth Sciences, Guilin University of Technology, Guilin, China, [3]Yunnan Earthquake Agency, Kunming, China

OPEN ACCESS

Edited by:
Daoyang Yuan,
Lanzhou University, China

Reviewed by:
Yueren Xu,
China Earthquake Administration, China
Jiawei Pan,
Chinese Academy of Geological Sciences (CAGS), China

***Correspondence:**
Lichun Chen
glutclc@glut.edu.cn

Specialty section:
This article was submitted to Structural Geology and Tectonics, a section of the journal Frontiers in Earth Science

Received: *21 December 2021*
Accepted: *24 February 2022*
Published: *06 April 2022*

Citation:
Li Y, Chen L, Ran Y and Chang Y (2022) Microscopic Characteristics of Fault Gouge in Minor-Surface-Rupture Faults: A Case Study in the Longmenshan Fault Zone, Eastern Tibetan. Front. Earth Sci. 10:840667. doi: 10.3389/feart.2022.840667

Active faults with potential earthquake magnitude of 6–7 are often incorrectly identified as non-Holocene active faults by traditional geological methods because their co-seismic displacements were very small or even did not reach to surface, and are defined as minor-surface-rupture faults. Geological studies associated with the 2013 Lushan Ms 7.0 earthquake show that the Dachuan–Shuangshi fault (DSF) in the southern segment of the Longmenshan fault zone (LFZ) is a minor-surface-rupture fault. This study focuses on the microstructure and mineral composition of the fault gouge in the DSF using optical microscopy, a scanning electron microscope (SEM), and X-ray diffraction (XRD) methods; then, we compare our results with the previous achievements in the Beichuan–Yingxiu fault (BYF), a major seismogenic fault of the 2008 Wenchuan earthquake, in the middle–northern segment of the LFZ. The results show that the microscopic characteristics of the fault gouge of the DSF are obviously different from those of the BYF in the following aspects: 1) the thickness of the fault gouge produced by one fault event is less than 5 mm; 2) under the microscope, no obvious micro-cracks were examined in surrounding rocks around the fault gouge, and discontinuous micro-cracks and untypical S-C fabrics in the fault gouge were observed; 3) under the SEM, reworked fragments were rare in the fault gouge; 4) the XRD mineral analysis reveals that the total clay content is less than 50%, the content of kaolinite is obviously higher than that of clinochlore, and the content of illite/smectite mixed layer is less than 30%. A contrastive analysis reveals the differences between the microscopic features of the fault gouge of the DSF and the BYF, which are systematical. Therefore, the abovementioned microscopic characteristics identified from the fault gouge in the DSF may be used as auxiliary indicators to identify minor-surface-rupture faults.

Keywords: fault gouge, microstructure, mineralogical composition, minor-surface-rupture fault, southern Longmenshan fault zone

INTRODUCTION

The offsetting and overlying relationship between faults and Late Quaternary strata is the most immediate evidence to identify the age of fault activity. According to the present achievement, the fault that does not offset the Late Pleistocene or Holocene strata is unlikely to trigger earthquakes with surface ruptures in the future. Although some faults could offset the surface, their co-seismic displacements are very small, only a few centimeters to a few tens of centimeters, and the remains can easily be eroded, and hardly be preserved and identified in the geological record. For example, the 2013 Lushan Ms 7.0 earthquake that occurred along the southern segment of the Longmenshan fault zone (LFZ) did not produce obvious surface rupture (Li C. et al., 2013; Xu et al., 2013a; Xu et al., 2013b; Lei et al., 2014). Such type of active faults is classified as minor-surface-rupture active fault (Chen et al., 2013a), and by traditional geological methods, they are easily identified as non-Holocene active faults, which leads to the neglect of the future strong earthquake risk along these faults.

The fault gouge is the direct lithological product of the fault activity and is formed *via* relatively complex physical and chemical processes related to the low-grade metamorphism that accompanies fault slip (Bos et al., 2000). Thus, the microstructure of the gouge contains information on the fault slip and behavior as well as the nature of the physical and chemical environment during faulting (Reinen, 2000; Zhang et al., 2002; Yuan et al., 2013). Although, so far, no explicit relationship between the microstructures of the fault gouge and the intensity of seismic activity has been reported, we can still find some implications and study cases from the observation of the fault gouge microstructures of the known minor-surface-rupture active faults and the comparison with those of intense active faults.

Geological observations show that the seismic activity of the southern segment of the LFZ is obviously weaker than that of the middle–northern segments, and the Dachuan–Shuangshi Fault (DSF), the unique fault in the southern segment with evidence of Holocene offset, is considered as a minor-surface-rupture fault (Yang et al., 1999; Densmore et al., 2007; Chen et al., 2013b; Wang

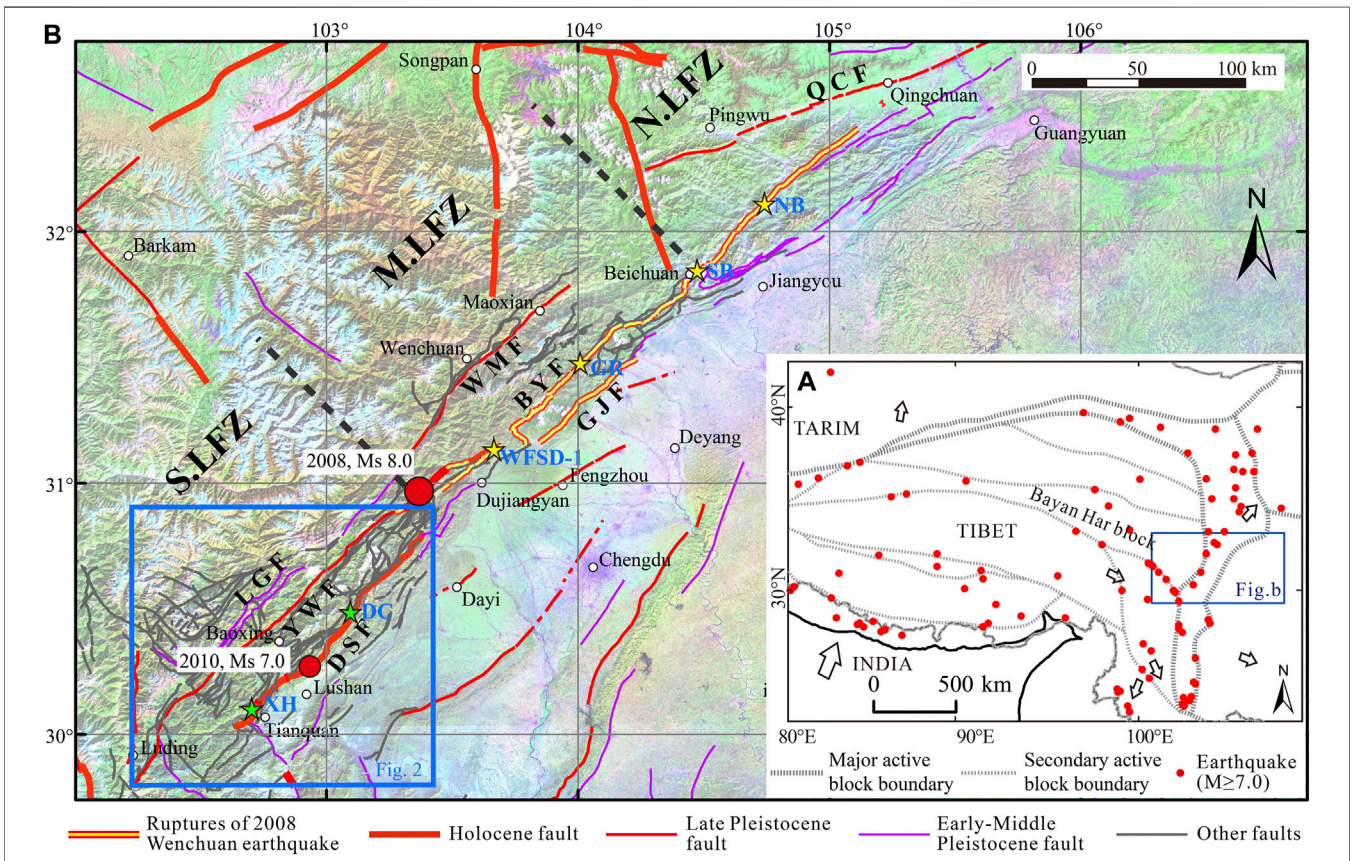

FIGURE 1 | Map showing **(A)** the location of the study area in Southwest China, along with the tectonic setting and major earthquake ($M \geq 7$) epicenters in the Tibetan Plateau (arrows denote movement directions of active blocks), **(B)** segmentation of the Longmenshan fault zone (LFZ) and other faults; N. LFZ, M. LFZ, and S. LFZ denote the northern, middle, and southern segments of the LFZ, respectively. Fault names: XKDF: Xinkaidian, SYF: Shiyang, DSF: Dachuan-Shuangshi, YWF: Yanjing–Wulong, LGF: Longdong–Gengda, GJF: Guanxian–Jiangyou, BYF: Beichuan–Yingxiu, WMF: Wenchuan–Maoxian, and QCF: Qingchuan. Green and yellow stars denote the fault gouge sampling sites from this study and previous research, respectively, XH: Xiaohe, DC: Dachuan, WFSD-1: Wenchuan Earthquake Fault Scientific Drilling Hole-1 (Li H. et al., 2013; Si et al., 2014; Wang H. et al., 2014; Chen et al., 2016; Liu et al., 2016), GR: Golden River (Duan et al., 2016), SB: Shaba (Yuan et al., 2013), and NB: Nanba (Han et al., 2010).

et al., 2013; Chen et al., 2014; Dong et al., 2017). We have found fault gouges from the outcrop and drill holes along the DSF. Furthermore, the 2008 Wenchuan Ms 8.0 earthquake that occurred along the middle–northern segments of the LFZ produced significant surface-rupture zones with a total length of more than 300 km (**Figure 1B**) (Xu et al., 2009). An abundance of gouges was observed at the surface ruptures, and the microstructures of these gouges have recently been investigated (Fu et al., 2008; Han et al., 2010; Yuan et al., 2013; Yuan et al., 2014). In particular, the "Wenchuan Earthquake Fault Scientific Drilling" (WFSD) project collected a large volume of fault gouge samples from borehole cores, again providing valuable microstructural information (Li H. et al., 2013; Si et al., 2014; Wang et al., 2014; Chen et al., 2016; Liu et al., 2016).

This study presents an analysis of the microstructure and mineral composition of the fault gouge samples collected along the DSF in the southern segment of the LFZ. We compared our results with results from the middle–northern segments of the LFZ to provide evidence and study case regarding differences between less-intense and intense active fault, and then benefit for identifying the minor-surface-rupture by the fault gouge microanalysis.

LATE QUATERNARY SURFACE ACTIVITY OF THE SOUTHERN SEGMENT OF THE LFZ

The LFZ is over 500 km long and forms the eastern boundary of the Bayan Har Block in the Tibetan Plateau. In general, the fault zone is divided into the southern, middle, and northern segments, bounded by the Yingxiu town of Wenchuan County and Beichuan County (**Figure 1B**). The fault zone is 30–50 km wide, with an overall trend of NE 30°, and dips toward the NW at 50–80°. The fault zone consists of several imbricate thrust faults with strike-slip components that are roughly parallel and known as the back-range, central, fore-range, and range-front (buried) faults (Zhang et al., 2008). The geometry of the LFZ is relatively simple in the middle–northern segments, but branches into a series of roughly parallel fault sets toward the south. Here, the fault zone intersects other NW-trending faults near the Baoxing County and further diverges to the NW and SE, with the width increased to about 80 km (**Figure 1B**) (Chen et al., 2013b; Chen et al., 2014).

The geomorphological analysis suggests that differential uplift in the southern segment of the LFZ is noticeably weaker than that in the middle–northern segments (Gao et al., 2016). The southern segment consists of moderately elevated mountains, with few Quaternary basins. Structurally, this area consists of a series of subparallel NE-striking faults and arc-like thrusts, which can be recognized from local linear features in satellite imagery. In the southern segment of the back-range fault, also referred to as the Gengda–Longdong Fault, there is no evidence of the Late Quaternary activity. Geological surveys have shown that the southern segment of the central fault (the Yanjing–Wulong Fault) may have been active in the early part of the Late Pleistocene (Chen et al., 2013b). The range-front fault is mostly buried in the southern segment, and no geological profile showing offsets of Late Pleistocene–Holocene lithologies was found. However, traces of active folds do appear, and they are inferred to represent a buried fault system active since the Late Pleistocene that does not reach the surface (Xu et al., 2013b; Dong et al., 2017).

The southern segment of the aforementioned fore-range fault is dominated by thrusting and is known as the DSF. The fault extends from the northeast of Dayi County in the north to the southwest of Tianquan County in the south, with a length of over 115 km, trending at NE 40° and dipping toward the NW (**Figure 2**). Several trenches along the DSF show that it has offset Holocene strata, with a co-seismic vertical displacement of ~0.3 m, and with unclear fault planes. Therefore, the DSF is classified as a minor-surface-rupture fault (Densmore et al., 2007; Chen et al., 2013b; Chen et al., 2014; Dong et al., 2017).

MICROSTRUCTURE AND MINERALOGICAL COMPOSITION OF FAULT GOUGE IN THE DSF

Sampling and Methods

The DSF, the unique fault with evidence of the Holocene offset in the southern segment of the LFZ, extends through the township of Dachuan, Lushan County. Based on previous seismic surveys, six boreholes (DC1–DC6) were drilled at this site (site DC in **Figures 1B**, **2**). As shown in **Figure 3**, boreholes DC4, DC5, and DC6, located on the hanging wall of the fault, penetrate the fault plane and reveal two fractured sections. Borehole DC4 (30.4876°N, 103.1023°E) reveals a fault fracture zone at depths of 41.8–75.5 m, consisting predominantly of cataclastic sandstone or conglomerate and cataclasite rock, with a soft fault gouge of 1 cm thickness at a depth of 60.3 m that is gray-white in color and dips at 60°. Another fracture zone with evidence of compressional and folded deformation is observed at depths of 90.7–97.7 m. In borehole DC5 (30.4891°N, 103.1029°E), the two fractured sections are at depths of 98.2–99.5 m and 103.6–108.0 m, respectively. Oriented rock fragments and cataclastic, lens-like, and schistose fabrics were observed in the two fractured zones, which dip up to 70°. Borehole DC6 (30.4901°N, 103.1038°E) revealed one fractured section at a depth of 91.9–96.6 m and another at 103.0–104.5 m. The uppermost section also contains noticeable cataclasis, lenses, and schistosities, with clear compression surfaces and a thin fault gouge that dips at 65–70°. The lower section is characterized by coal beds with folds. Fault gouge samples were collected from these two sections, as shown in **Figure 3** and **Table 1**.

A very clear fracture zone is also evident in the DSF on a slope west of Xiaohe town, Tianquan County. At an abandoned limestone quarry pit (site XH in **Figure 1B**, **2**; 30.1079°N, 102.7243°E), the fracture zone is composed of a fault gouge, fault breccia, cataclasites, and folds. The fault gouge is loose with slightly variable thickness (20–50 cm) at different locations, and the fault is exposed at the surface, which implies an activity in the Late Quaternary; the exposed fault trace dips toward 300° at 65–75°. The hanging wall consists of Lower Permian limestone,

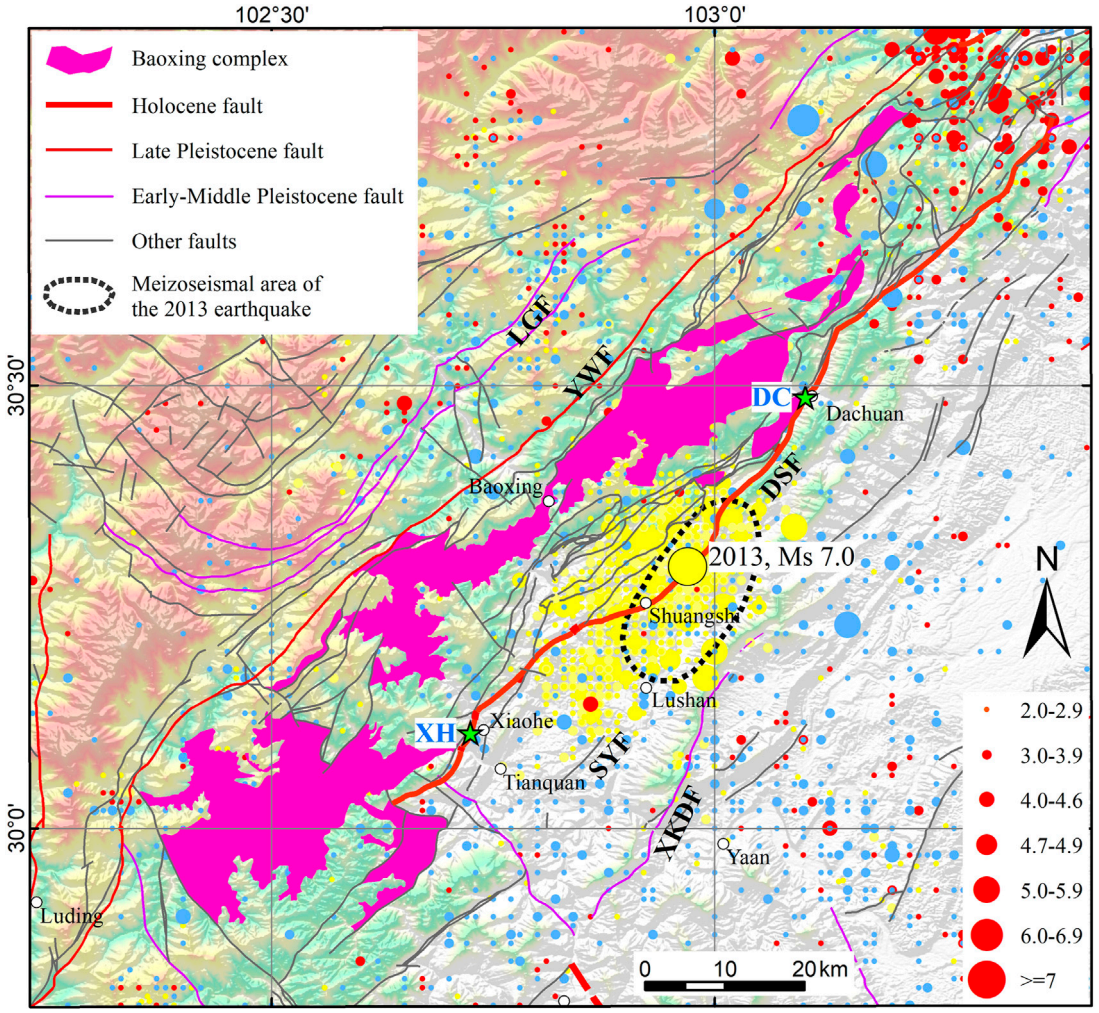

FIGURE 2 | Map showing the topographic distribution of the southern segment of the LFZ and earthquake epicenters ($M \geq 2.0$). The blue circles denote events before the 2008 Wenchuan earthquake, red circles denote events after the 2008 Wenchuan earthquake but before the 2013 Lushan earthquake, and yellow circles denote relocated aftershocks of the 2013 Lushan earthquake. Fault names: XKDF: Xinkaidian and SYF: Shiyang (see **Figure 1** for other symbolic meanings).

and the footwall consists of Upper Permian basalt. Samples of this fault belt were collected (**Figure 4**; **Table 1**).

Fault gouge samples were processed according to the method adopted by Tanaka et al. (2001). Each sample was carved into four slabs (for preservation, mineralogical sampling, hand specimens, and thin sections). The thin sections of the core samples from the Dachuan site were made by cutting parallel to the long axis of the core and perpendicular to the fault plane. For the outcrop samples from the Xiaohe site, the cuts were made perpendicular to the strike and plane of the fault. Then the thin sections were examined by optical microscopy (**Figures 5**–**7**), with selected samples analyzed by a scanning electron microscope (SEM) (**Figure 8**).

To investigate the mineralogical composition of the fault gouges, X-ray diffraction (XRD) was used in this study. XRD analyses for the bulk-rock relative mineral content and semi-quantitative analyses for clay minerals were performed with a Dmax X-ray powder diffractometer (12 kW, 45 kV, and 100 mA) at the Beijing Micro Structure Analytical Laboratory at Peking University Science Park. Unoriented powder bulk samples were scanned with 2θ ranging from 3° to 45° with a step size of 0.02° by CuK-α radiation (0.15418 nm) and a scan rate of 2°/min. The relative amount of bulk clays in the bulk powder sample was evaluated, the proportions of which were further determined by analyzing the centrifugation-separated clay-sized portion (b2 μm). The clay-water slurry was air-dried on glass slides, and ethylene glycol was added to detect swelling components. Then the samples were heated to 550°C to distinguish kaolinite from chlorite.

Microstructural Observations

Dachuan Borehole Site

Sample DC4-1

Photographs taken under a stereoscope show that the fault gouge between the two walls of the fault (sandstone W1 and mudstone W2) occurs in three different colors: gray-black (X2), gray (X3),

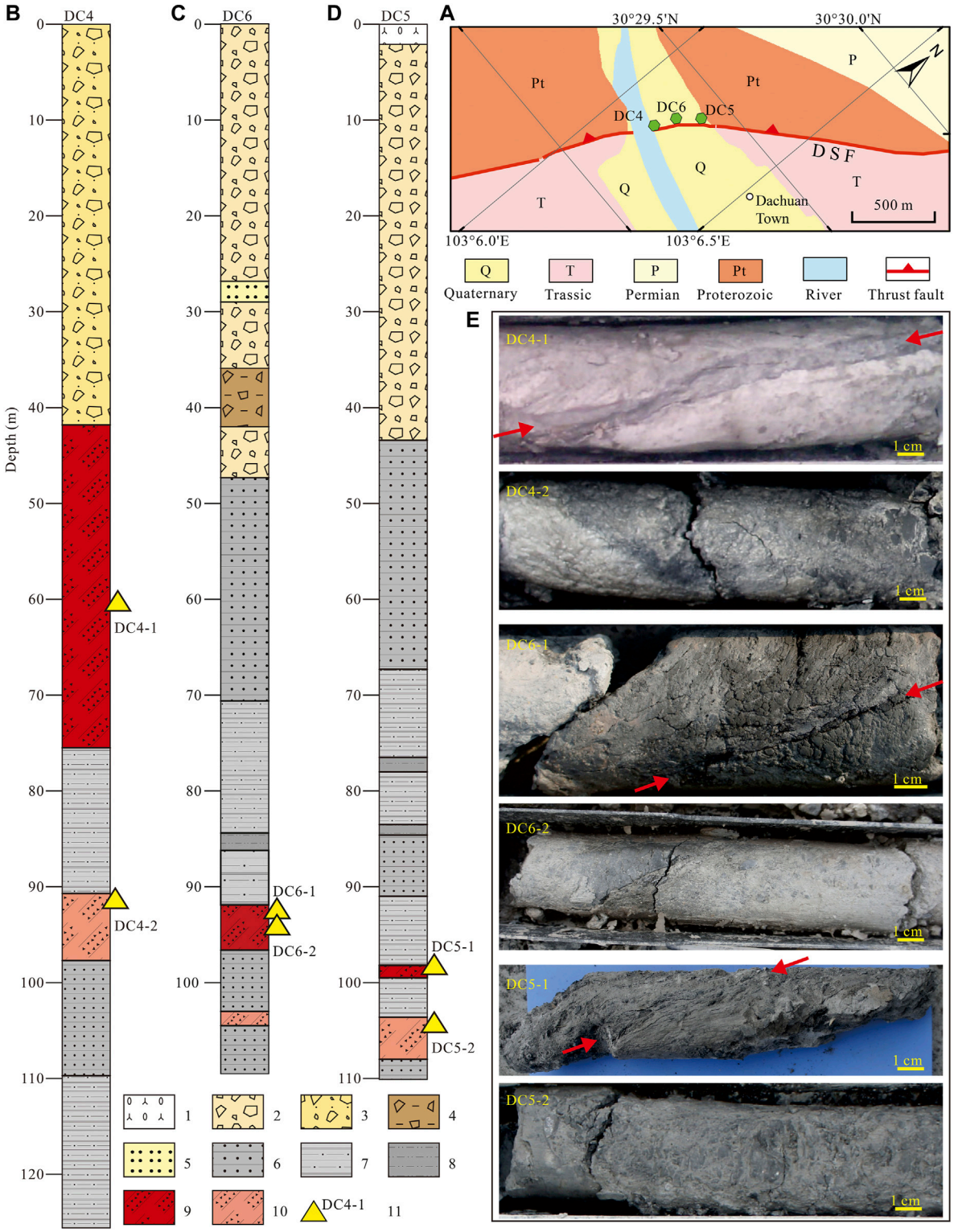

FIGURE 3 | (A) Geological map showing the borehole positions (green dots) at the Dachuan site (DC in **Figure 1B** and **Figure 2**) relative to the DSF. **(B–D)** Core logs of boreholes DC4, DC6, and DC5. Legends: 1: artificial soil fill, 2: boulder, 3: gravel intercalated with clay, 4: sandy gravel, 5: sand bed, 6: sandstone, 7: fine sandstone, 8: silty sandstone, 9: active fault belt, 10: old fault fracture belt, and 11: sampling site and number. **(E)** Photographs of core samples with red arrows showing locations of localized, soft, and thin fault gouge in fractured zones.

TABLE 1 | Descriptions of fault gouge samples from the DSF.

Sampling sites	Sample number	Description of samples
Dachuan site	DC4-1	From depths of 60.2–60.4 m in borehole DC4 and the upper fracture belt, with visible ~1-cm-thick loose soft fault gouge and detrital rock on either side
	DC4-2	From depths of 91.4–91.6 m in borehole DC4 and the lower fracture belt, with detrital rock intercalated with coal beds
	DC5-1	From depths of 98.2–98.4 m in borehole DC5 and the upper fracture zone, with broken cataclastic mudstone and thin layers of loose soft fault gouge
	DC5-2	From depths of 105.1–105.3 m in borehole DC5 and the lower fracture belt, with detrital rock
	DC6-1	From depths of 92.7–92.9 m in borehole DC6 and the upper fracture belt, with broken cataclastic mudstone and 3–5-cm-wide loose soft fault gouge
	DC6-2	From depths of 94.7–94.9 m in borehole DC6 and the upper fracture belt, with broken cataclastic mudstone
Xiaohe site	XH1	From cataclastic bedrock in the hanging wall of the fault and ~6 cm from the interface of the fault gouge belt
	XH2	From cataclastic country rock in the hanging wall of the fault, contacting with the fault gouge
	XH3	From the fault gouge and ~2 cm from the boundary between the fault gouge belt and hanging-wall cataclastic bedrock, as gray-white fault gouge
	XH4	From near the center of the fault belt (slightly closer to the footwall) and as gray-white fault gouge, with schistosity oblique to the slip plane
	XH5	From the gray-black breccia belt in the footwall of the fault, contacting with the fault gouge, with compressive schistosity visible
	XH6	From the gray-black breccia belt in the footwall of the fault and ~8 cm from the interface of the fault gouge belt

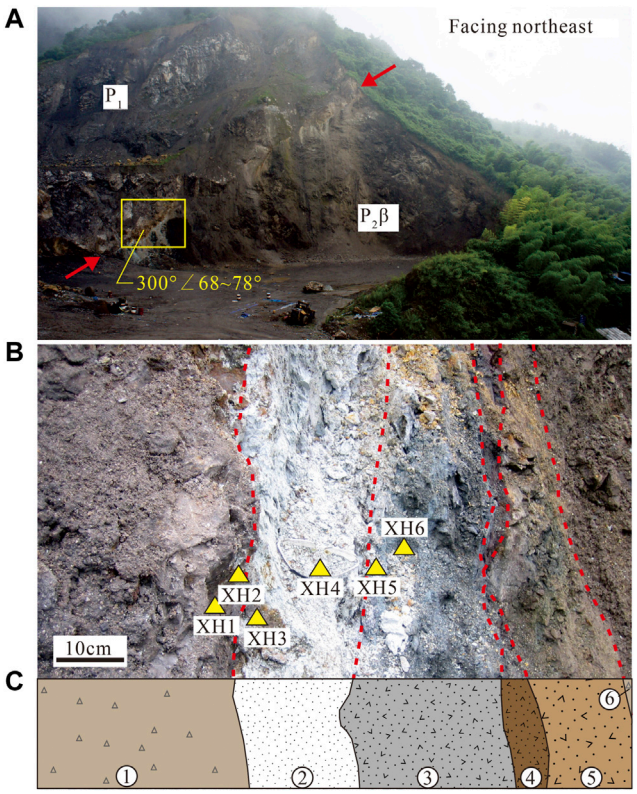

FIGURE 4 | (A) Photograph of the Xiaohe site (location shown in **Figure 1B**) with the fault trace denoted by red arrows. P_1: Lower Permian limestone and $P_2\beta$: Upper Permian basalt. The sampled area is shown by the yellow box, which is enlarged in **(B)** and contains the fault gouge sample sites XH1–XH6 (yellow triangles). **(C)** Interpretation of the fault belt. ① Cataclasite at the hanging wall, ② gray-white fault gouge, ③ gray-black fault breccia, ④ ferruginous vein, ⑤ yellow breccia, and ⑥ cataclasite at the footwall.

and light-gray (X4). The gouge zone is 2.5 cm thick, of which X2, X3, and X4 are 0.5–1.0, ~10, and ~15 mm, respectively (**Figures 5A,B**). Under an optical microscope, no obvious microscopic deformation structures were observed in walls W1 and W2 (**Figures 5C,D**). In fault gouges X2, X3, and X4, there were a series of subparallel and discontinuous fracture cleavages; of these, the scale and intensity in gouge X2 were greatest, followed by X3 and then X4. Inside these fault gouges, pores and fissures likely related to fluid migration were observed, and some pores developed in the solution seams (**Figures 5E–G**). Under the SEM, the boundary between the fault gouge and the sandstone cataclasite was obvious. The fragments, appearing principally as long angular strips, were mainly quartz grains with rare ilmenite and microcline. In the sandstone cataclasite, the debris was mostly larger than 20 μm and not arranged, and no second deformation or fracture was observed. On the boundary between cataclasite and the gouge, the particles were significantly reduced and generally smaller than 15 μm, the amount of clay increased, and the fragments were oriented and mostly clean and intact, with tiny amounts of clasts seen as reworked micro-cracks, or fragments (**Figures 8A,B**). Inside the gouge, particles larger than 15 m were rare, fine grains were oriented (**Figure 8B**), and micro- to nanometer-sized grains were observed (**Figure 8C**).

Sample DC4-2

This sample contains black and light-gray fault gouges with stripe-like features and clear edges. The parent rock of the black gouge is coal, and that of the light-gray gouge is mudstone. A series of discontinuous cracks are present in the light-gray fault gouge, parallel to the long-axis of the drill core (arrows in **Figures 5H,I**). Cracks healed by calcite can be occasionally observed along the fault (**Figure 5H**).

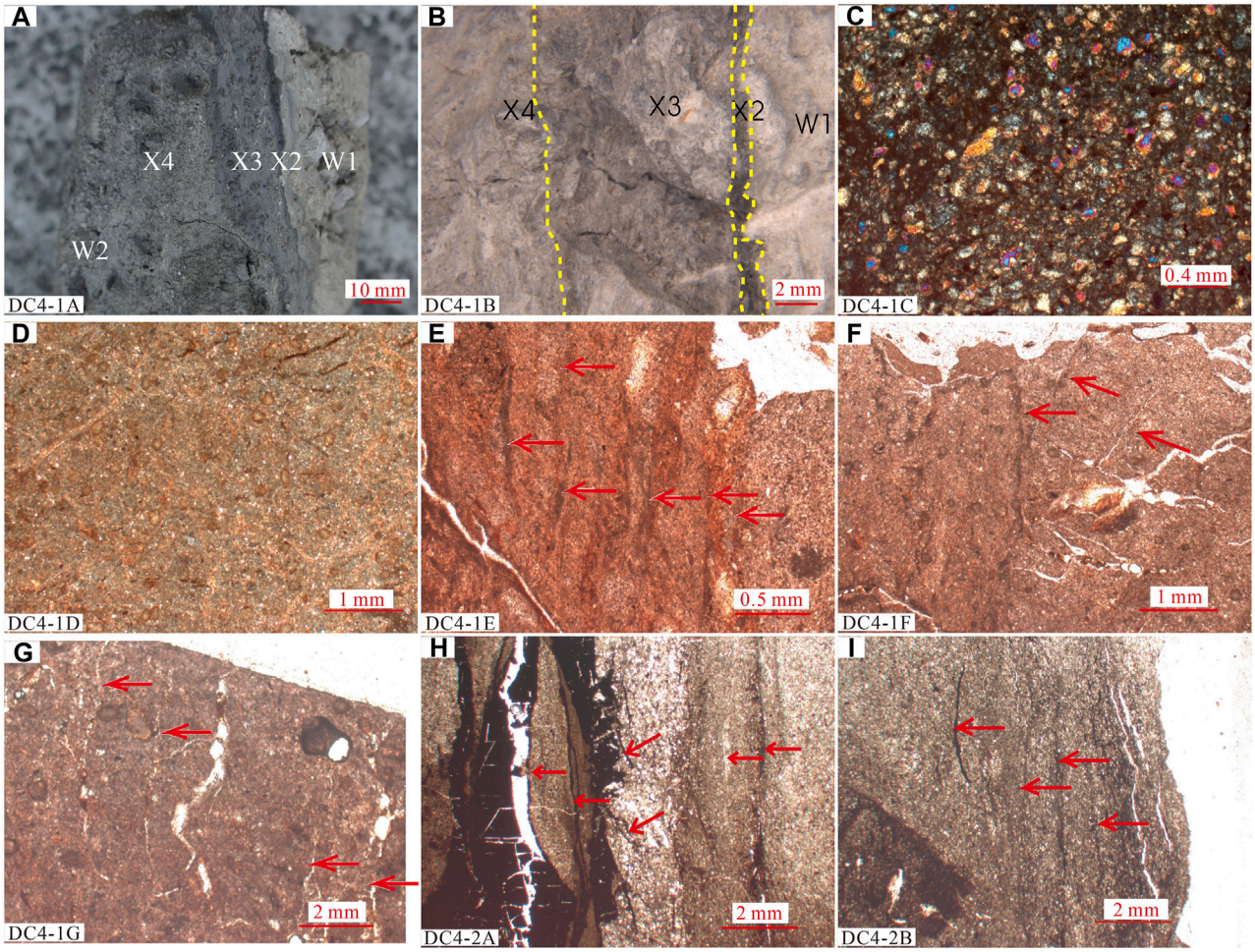

FIGURE 5 | Photographs of sample DC4-1 and DC4-2. **(A)** Core sample containing fault gouges X2, X3, and X4. W1 and W2 denote the country rock (sandstone and mudstone, respectively) on either side of the gouge. **(B)** Stereoscopic image showing the fine textures of the fault gouge samples X2, X3, and X4. **(C,D)** Photomicrograph of country rock W1 and W2, respectively, showing the lack of deformation. **(E–G)** Photomicrographs of sample DC4-1. **(H,I)** Photomicrographs of sample DC4-2. Arrows show discontinuous fracture cleavage or fissures.

Sample DC5-1

The fault gouge in DC5-1 contains en echelon fold structures, which are presumably formed under compression, and a quasi-S-C fabric (letters "S" and "C" in **Figure 6A**). This sample also contains discontinuous fracture cleavage (arrows in **Figure 6B**) and straight, fine striations (arrows in **Figure 6C**). As shown in **Figure 6D**, the debris and mineral fragments between the mudstone and fine sandstone show a strong orientation, indicating the sharply defined fault contact. Structural deformation is concentrated in the mudstone on the left, with two periods of activity being evident (arrows F1 and F2 in **Figure 6D**); F2 is cut by F1 at an inclination of ~30°. In addition, pressure solution seams can be observed locally in this sample (**Figure 6A**).

Sample DC5-2

This fault gouge also has an irregular, striped appearance with quasi-S-C fabrics (letters "S" and "C" in **Figure 6E**). Some of this S-C fabric folded during a compression event (**Figure 6F**).

Sample DC6-1

This gouge comprises two main colors, gray-black and light gray, and also displays a striped appearance. This feature is indicative of the newer fault trace, which is distinct and straight, at the interface of the two sets of gouge (**Figure 6G**). In the gray-black gouge, there are many subparallel fracture cleavages (arrows in **Figure 6G**), which transect the black stripes and intersect the newer fault plane at an angle of ~18°. In the light gray gouge, there

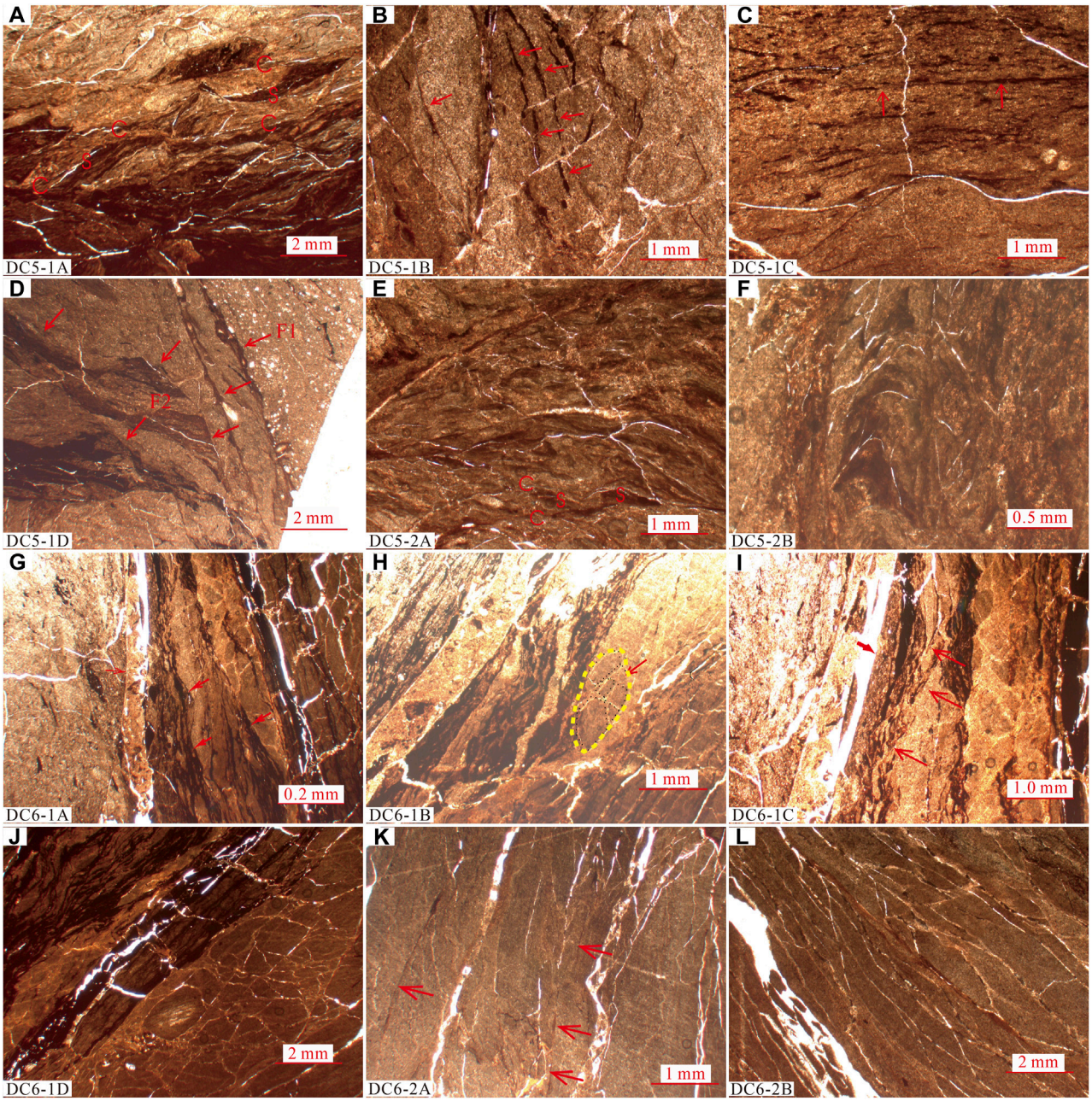

FIGURE 6 | Photomicrographs of samples DC5-1 **(A–C)**, DC5-2 **(D–F)**, DC6-1 **(G–J)**, and DC6-2 **(K,L)**. S and C denote quasi-S-C fabrics, and arrows indicate cracks or fracture cleavage. Yellow dashed lines mark reworked clasts.

are some mortar textures, with the long axis being subparallel to the fault plane (**Figure 6H**). Both sets of the fault gouge contain cracks, of which the density in the light gray gouge is higher than that in the gray-black gouge (**Figures 6I,J**).

Sample DC6-2

This sample comprises the fault gouge formed in mudstone and is light gray in color. Simple deformation is evident, with subparallel but discontinuous fracture cleavage (**Figure 6K**) or dense subparallel fissures (**Figure 6**L).

Xiaohe Outcrop Site

Sample XH1

Microscopic observation of this gouge reveals only minor cataclasis of mineral grains, with no preferred orientation or arrangement of long axes visible (**Figure 7A**).

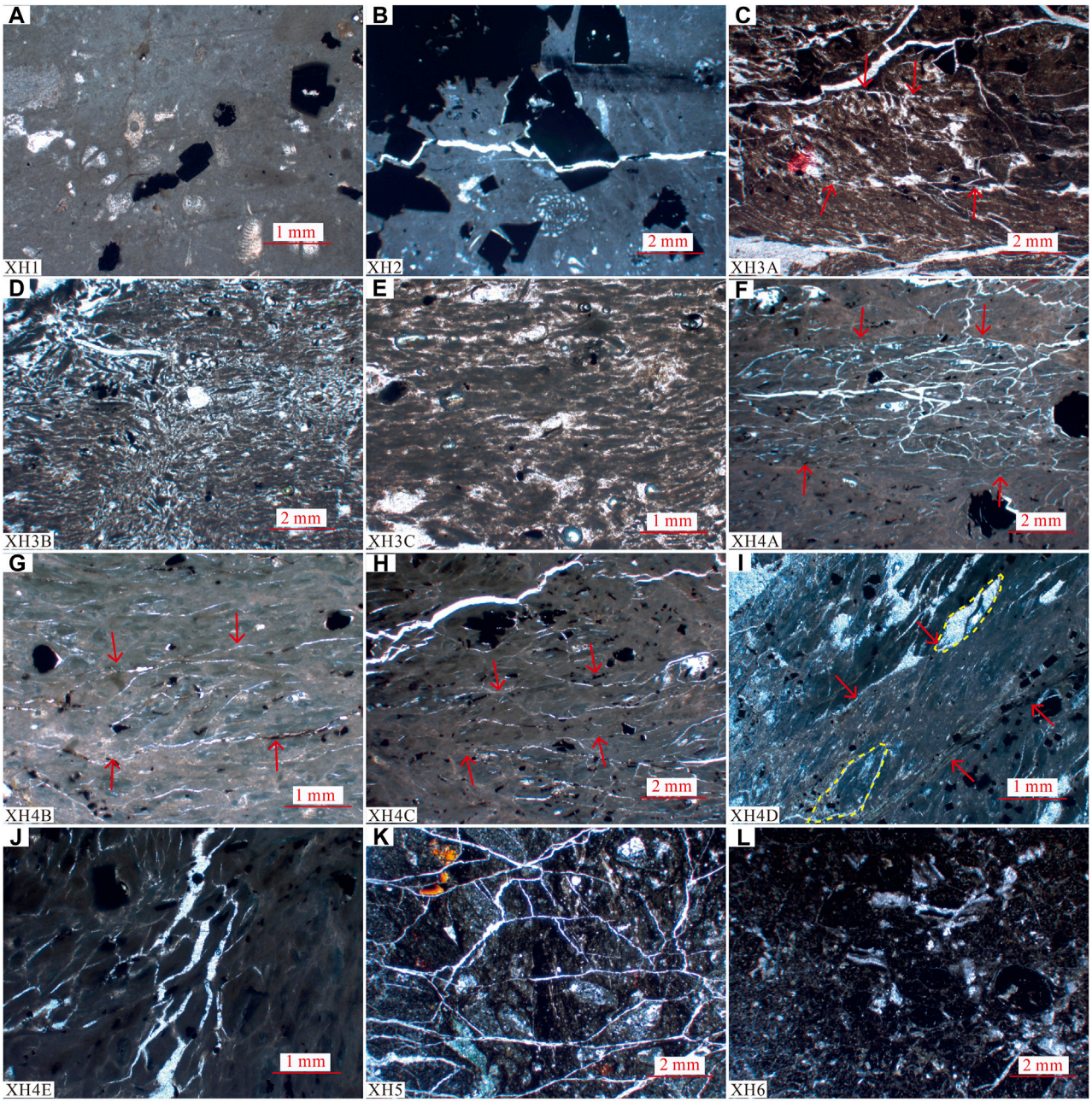

FIGURE 7 | Typical photomicrographs of samples from the Xiaohe site showing details of the microstructures. **(A)** XH1. **(B)** XH2. **(C–E)** XH3. **(F–J)** XH4. **(K)** XH5. **(L)** XH6. Arrows denote individual straight cracks and the localized deformation zones delimited by them.

Sample XH2

This gouge contains relatively long but irregular and unfilled cracks that transect sheet-like mineral grains locally (**Figure 7B**).

Sample XH3

This sample contains numerous sets of cracks and foliations (**Figures 7C–7E**), the broadest of which are filled with calcites, thus forming vein-like textures. The cracks are mostly disordered and v are not individually pervasive. Only two cracks (arrows in **Figure 7C**) are relatively straight, but are not very long, and bound by a domino-like structure consisting of rock fragments. The two sets of cracks mentioned before constitute a quasi-S-C fabric. In addition, it was observed that preexisting foliations were deformed by later cleavage in which mineral grains were oriented, with disorderly mineral arrangement at the intersection of the two foliations (**Figure 7D**). Pores and healed fissures related to fluid migration were observed (**Figures 7C–E**).

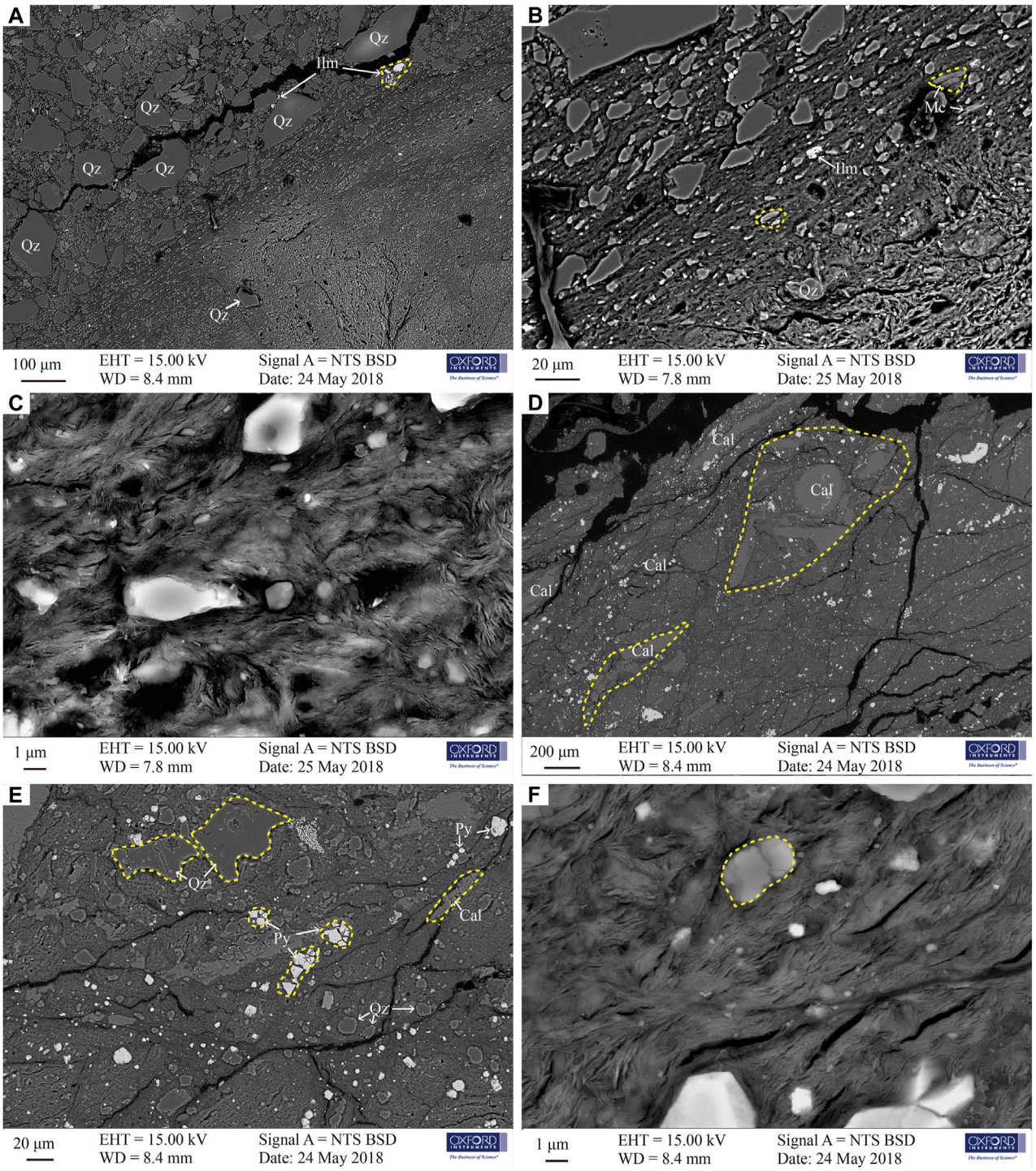

FIGURE 8 | Scanning electron microscope (SEM) images of the fault gouge samples DC4-1 **(A–C)** and XH4 **(D–F)**. Qz, quartz; Ilm, ilmenite; Cal, calcite; Mc, microcline; and Py, pyrite. Yellow dashed lines mark reworked clasts.

Sample XH4

Under an optical microscope, this sample has a much denser distribution of foliations and cracks than sample XH3. In addition, porphyroclasts, cataclastic minerals, and porphyrotopes are present in the microstructure. **Figure 7F** shows a zone of crack concentration that is limited by two straight cracks, outside of which several oblique fissures form a quasi-S-C fabric in conjunction with the principal foliations. As

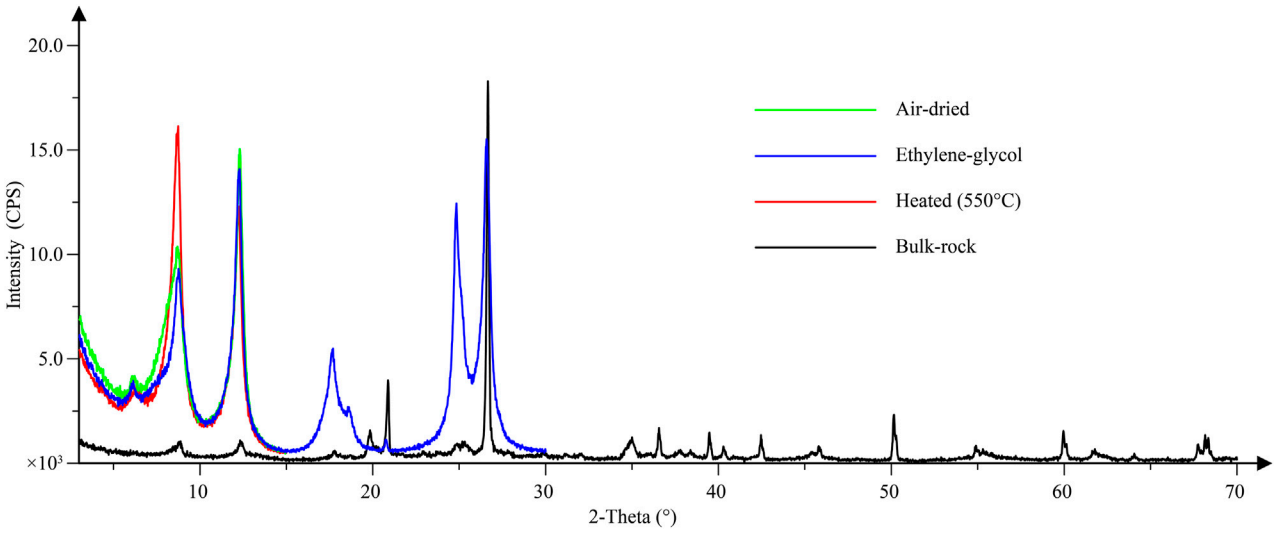

FIGURE 9 | Graph showing the XRD patterns of sample DC4-1.

shown in **Figure 7G**, there are rock fragments bounded by two straight cracks, which overall constitutes a domino-like fabric. These cracks intersect the principal foliations at low angles with evidence of cataclastic mineral grains (**Figure 7H**). **Figure 7I** displays numerous foliations and quasi-S-C fabrics in which debris is delimited by two straight cracks, forming an oriented domino-like fabric. In addition, some fragments are reworked and show fractures or micro-cracks. As shown in **Figure 7J**, the preexisting foliations are transected by quite broad younger cracks that contain replacement filling of calcite and intersect the foliations at high angles. Pores and fissures possibly related to fluid migration can be observed in this gouge, and pores are occasionally developed in the healed fissures (**Figures 7F–I**). According to the SEM observation, the fragments in sample XH4 are mainly composed of calcite, quartz, and pyrite, and the directional arrangement and reworked deformation or fragmentation are obvious. Calcite grains, which are most abundant, are large and mainly vein-shaped. Compared with the calcite, the quartz and pyrite particles are smaller (generally <20 μm), subangular, and irregular in shape. The phenomenon of clasts being wrapped by clay is apparent, and micro- to nanometer-sized grains could be observed (**Figures 8D–F**).

Sample XH5

This sample also contains preexisting foliations transected by later cracks, along with cataclastic rocks, and relatively straight but branching cracks (**Figure 7K**).

Sample XH6

Almost no deformation is visible in the microstructure of this sample, but several fissures or some cataclasites are evident (**Figure 7L**).

Overall, the country rock samples from the Xiaohe site display very little deformation in their microstructure, while inside the fault gouge, sample XH4, collected from near the center of the fault, shows relatively abundant deformation concentration.

Mineralogical Results From XRD Analyses

XRD mineralogical analyses were performed on the fault gouge from core sample DC4-1 and outcrop sample XH4, based on the abovementioned microstructural observation results.

As shown in **Figure 9** and **Table 2**, the mineralogical analysis identified quartz and clays as the major minerals, which reach contents of 49% and 44%, respectively, for the fault gouge of sample DC4-1. In addition, small amounts of albite and microcline were detected. The clay in sample DC4-1 is composed of illite, and mixed layers of illite/smectite, kaolinite, and clinochlore, and no dissociative smectite was found. Among these clay minerals, the content of illite is the highest (39%), followed by mixed layers of illite/smectite, and the clinochlore content is lowest at 13%. The ratio of the illite/smectite mixed layer is only 15%.

Fault gouge sample XH4 has a richer variety of minerals than sample DC4-1, including clay, calcite, quartz, pyrite, and small amounts of albite, microcline, and gypsum. The content of calcite is higher (~29%) than that of quartz (~16%), but clay content is 36%. The clay minerals, similar to that in sample DC4-1, are composed of illite, mixed layers of illite/smectite, kaolinite, and clinochlore. No dissociative smectite was found. Of the clay minerals present, illite has the highest content, reaching 50%, followed by the mixed layers of illite/smectite, and the clinochlore content is lowest at only 6%. The ratio of the illite/smectite mixed layer is also 15% (**Figure 10** and **Table 3**).

DISCUSSION

Slip Behavior of the DSF Revealed by Fault Gouge Microanalysis

Previous studies about experimental gouge and nature fault gouge have suggested that irregular striations, quasi-S-C fabrics, and

TABLE 2 | Bulk-rock and clay mineral compositions of fault gouge sample DC4-1.

Bulk composition (%)							
Quartz	Albite	Microcline	Calcite	Pyrite	Gypsum	Total clay	
49	3	4	—	—	—	44	
Clay composition (%)					Mixed-layer ratio (%S)		
Smectite	Illite/smectite	Illite	Kaolinite	Clinochlore	Clinochlore/smectite	Illite/smectite	Clinochlore/smectite
—	27	39	21	13	—	15	—

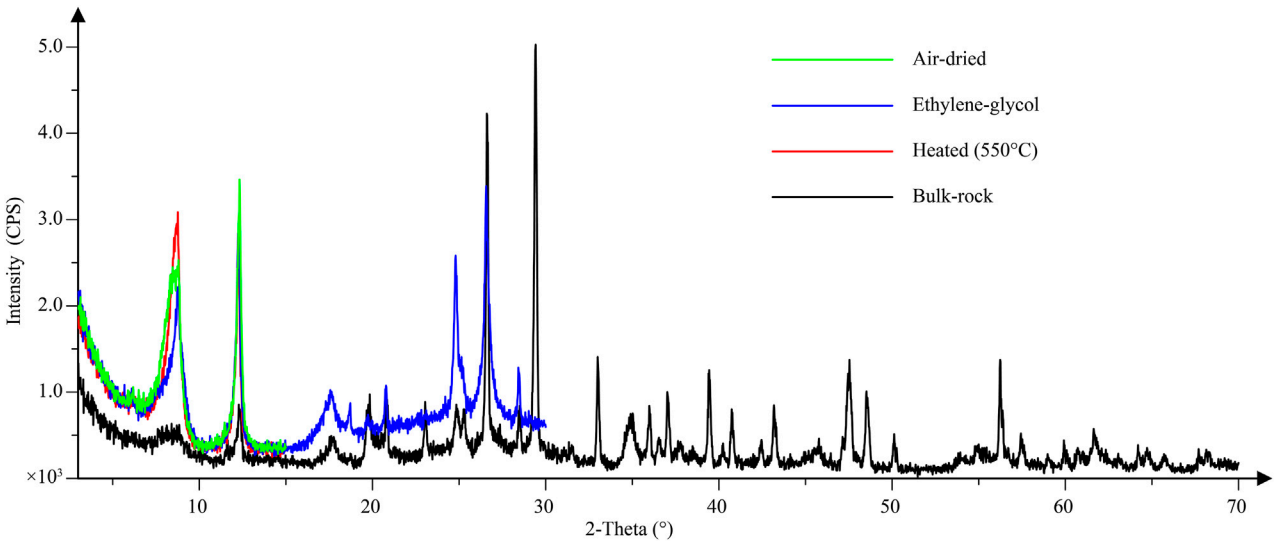

FIGURE 10 | Graph showing the XRD patterns of sample XH4.

TABLE 3 | Bulk-rock and clay mineral compositions of fault gouge sample XH4.

Bulk composition (%)							
Quartz	Albite	Microcline	Calcite	Pyrite	Gypsum	Total clay	
16	2	4	29	10	3	36	
Clay composition (%)						Mixed-layer ratio (%S)	
Smectite	Illite/smectite	Illite	Kaolinite	Clinochlore	Clinochlore/smectite	Illite/smectite	Clinochlore/smectite
—	28	50	16	6	—	15	—

small folds in the fault gouge are associated with fault creep, whereas localized brittle deformation features such as discontinuous fracture cleavages, straight cracks or striations, concentrated zones of cracking, and other deformation are caused by stick-slip during faulting (Moore et al., 1989; Reinen, 2000; Zhang et al., 2002; Yuan et al., 2013).

The microstructure observations mentioned before demonstrate that samples DC4-1, DC5-1, and DC6-1, collected from the upper fracture zone shown in the cores at the Dachuan site, have more abundant signs of deformation such as straight fracture planes, cracks or striations, subparallel fracture cleavage, and preferred orientations of porphyroclasts, and an overall higher degree of deformation than samples DC4-2 and DC5-2 (from the lower fracture zone). It can reasonably be concluded that the upper fracture zone has been the most recently active part of the DSF. Sample DC4-1 shows almost no microstructural deformation in the country rocks on either side of the fault gouge (**Figures 5C,D**). Thus, the structural deformation is concentrated in the ~2.5-cm-thick fault gouge in the center of the fracture zone (**Figures 5A,B**).

In the country rock on either side of the fault gouge at the Xiaohe site, samples XH1, XH2, XH5, and XH6 show little or no microstructural deformation, which is in sharp contrast to samples XH3 and XH4 within the fault gouge (**Figure 7**). In particular, XH4, which was collected from near the center of the fault gouge, has the most conspicuous fractures or micro-cracks, oriented fragments, and reworked clasts, which imply a decreasing trend of deformation from the center to either side of the fault plane. Such deformation is unevenly distributed, with a 1- to 5-mm-thick zone composed of cleavages or micro-cracks or domino-like arranged fragments bounded by two subparallel straight cracks, within which mineral grains or debris have a preferred orientation. Outside of this zone, only a few micro-cracks developed.

According to Han et al. (2010) and Duan et al. (2016), the newest fault gouge in a fault belt is the softest, thinnest, and deepest in color, with almost no breccia inside and a clear, flat boundary with other parts. Therefore, it can be speculated that the gray-black and relatively loose and soft gouge X2 with 0.5- to 1.0-mm thickness (**Figures 5A,B**) in sample DC4-1 and the localized brittle deformation zone bounded by two straight cracks in sample XH4 are the result of the most recent stick-slip event (**Figures 7F–I**).

Previous studies suggest that the illite-rich fault gouge is the product of the fault slip that occurs during an earthquake, whereas the smectite-rich fault gouge is the product of fault creep (Chen et al., 2007; Isaacs et al., 2007). In this study, relatively abundant illite contents were found in the fault gouge at both the Dachuan boreholes and the Xiaohe outcrop sites, and almost no smectite was present (**Tables 2**, **3**).

Stick-slip event of the fault is generally accompanied by co-seismic frictional heating, and experimental research works showed that the flash heating can cause thermal decomposition of minerals to form nanoparticles (Han et al., 2007). Then the existence of micro- to nanometer-sized grains can greatly reduce the friction strength of the fault and play a role of lubrication and drag reduction in the fault slip, enabling the fault slip in a large scale (Yuan et al., 2014). As mentioned before, abundant micro- to nanometer-sized grains were developed in the fault gouge of the samples DC4-1 (**Figures 8A–C**) and XH4 (**Figures 8D–F**).

Friction experiments show that the existence of water can lead to the transformation of frictional sliding from stable sliding to unstable sliding, which would result in seismic nucleation. Therefore, a more intense fluid activity in the fault gouge may correspond to more seismic events in the fault history (He et al., 2006; He et al., 2007; Han et al., 2010). Abundant pores could relate to fluid migration developed in the fault gouge in samples DC4-1 and XH4 from the two study sites.

Based on a combination of the microstructure observations and mineralogical analysis results, the DSF presents obvious stick-slip behavior and has the ability to produce devastating earthquake confirmed by paleoseismological studies (Densmore et al., 2007; Chen et al., 2013b; Chen et al., 2014; Dong et al., 2017). It should be pointed out, of course, that other mechanisms in addition to fault slip may involve the development of microstructures of our fault gouge. For example, the development of micro- to nanometer-sized particles observed in our fault gouge may involve thermal decomposition in parts, and the development of healed fluid migration fissures may relate to the pressure solution.

Differences Between DSF and BYF in Fault Gouge Microstructures and Mineralogical Composition

As shown in **Table 4**, features of the fault gouge of the DSF in the southern segment of the LFZ, as revealed by borehole and outcrop observations, differ significantly from observations made in trenches and drill-holes in the middle–northern segments. For instance, in the southern segment, the thickness of the fault gouge produced by single events is considerably less than that in the middle–northern segments, and the country rock is less fractured on a microscopic scale. Additionally, the fracture system in the southern segment is relatively simple and mainly consists of micro-cracks or discontinuous fracture cleavage. However, oriented fragments or clasts are distinct in the fault gouge from the southern LFZ, unlike in the fault gouge from the middle–northern segments in which reworked clasts are also evident.

With the exception of clay, the mineralogical composition of fault gouge does not seem to be comparable at study sites in the LFZ. The total clay content in the relatively new fault gouge in the middle–northern segments of the LFZ is generally more than 50%, or even more than 70% (Yuan et al., 2013; Wang et al., 2014; Duan et al., 2016), whereas that of our two study sites in the southern segment was only around 40%. In addition, the clay mineral composition in the fault gouge also differs significantly between the southern and the middle–northern segments. For example, the contents of the illite/smectite mixed layer and chlorite are significantly lower in the southern segment, whereas the content of kaolinite is significantly higher. The illite/smectite mixed layer ratio in the southern segment is significantly smaller than that in the middle–northern segments (**Tables 2**–**4**).

In terms of ductile deformation features, the microstructures of the fault gouge from the south segment of the LFZ is different from that from the middle–northern segments. For instance, the S-C fabric from the gouge of the middle–northern segments is relatively strong and obvious, while that from the gouge of the southern segment are very untypical and we call it the quasi-S-C fabric.

Previous research works on structural geology revealed that the DSF is unique in the southern segment of the LFZ because it contains records of Holocene offset at the surface (Densmore et al., 2007; Chen et al., 2013b; Chen et al., 2014; Dong et al., 2017). However, in contrast to the middle–northern segments of the LFZ, which show clear fracture surfaces and >1-m co-seismic displacement (Xu et al., 2009; Ran et al., 2010a; Ran et al., 2010b; Ran et al., 2013; Ran et al., 2014), the DSF produced only tiny offsets near the surface. Therefore, these studies suggested that, in contrast to middle–northern LFZ, the single faults in southern LFZ are less active and lead to lower seismic activity because they have more branches distributed over a larger area, allowing tectonic deformation to be

TABLE 4 | Comparison of fault gouge microanalysis results between the DSF and BYF.

		DSF	BYF
Fault gouge thickness of single fault event		0.5–1.0 mm* or 1–5 mm[#]	>10 mm[*,#,a,b,c]
Country rock around fault gouge		No notable trace of structural deformation* or a few discontinuous non-straight micro-cracks[#]	Many (micro-) cracks, diamond-like cracks or shear planes[*,#,b,d]; local severely fractured breccias, and widely distributed fissures[#,c]
Features of debris or mineral clasts		Oriented arrangement[*,#] or a few porphyroblastic features[#]	Obvious oriented arrangement, many dislocations of debris or mineral clasts[*,#,b,d,e]
Ductile deformation		Local features of quasi-S-C fabrics and small folds[*,#]	Strong S-C fabrics, notable P-foliations, extended debris grains, and asymmetric drag structures[*,#,a,b]
Total clay content		44%* or 36%[#]	~50% or higher[*,f,g] or 72.8%[#,b]
Clay mineral composition	Relative content	I > I/S > Kln > Chl[*,#]	I/S (~50%) > I > Chl (~30%) > Kln (almost 0%)[*,f,g], or I > I/S (40%) > Chl (>7%) > Kln (1%)[#,b,f]
	I/S mixed layer ratio	15%[*,#]	>50%[*,f,g] or 35%[#,b,f]

*Note: Symbol * denotes fault gouge (rock) from boreholes, and # is fault gouge exposed on the surface.*
[a]*Li et al. (2013b).*
[b]*Yuan et al. (2013).*
[c]*Han et al. (2010).*
[d]*Si et al. (2014).*
[e]*Chen et al. (2016).*
[f]*Wang et al. (2014).*
[g]*Duan et al. (2016).*
The sampling sites of those study are shown in ***Figure 1****. I: illite, I/S: illite/smectite mixed layer; Kln: kaolinite, Chl: clinochlore.*

accommodated by more faults (Densmore et al., 2007; Chen et al., 2013b; Chen et al., 2014; Dong et al., 2017). Coincidentally, the microstructure, clay content, and clay mineral content of the fault gouge varied greatly between the southern and middle–northern LFZ. That is, the results of our microanalysis of the fault gouge further support the inference that the southern segment of LFZ is not like the middle–northern segments and is unlikely to experience an *Ms* 8.0 or larger earthquake.

Implications to identify minor-surface-ruptures by microscopic analysis of fault gouge.

According to the comparison of the microscopic characteristics of the abovementioned gouges, whether collected from near the surface or from boreholes, it can be seen that the DSF with minor co-seismic displacement is systematically different from the BYF with intense activity. These differences may be caused by the intrinsic differences in the active characteristics of the two types of faults; that is to say, the information identified from the fault gouge of the DSF may serve as a preliminary marker for identifying minor-surface-rupture faults. To sum up, the obvious signs about fault gouge are as follows:

1) fault gouge thickness of a single fault event is less than 5 mm;
2) under a microscope, no obvious micro-crack was examined in surrounding rocks around the fault gouge; and observed micro-cracks are discontinuous and S-C fabrics are not very typical in the fault gouge.
3) under SEM, mineral debris reprocessing phenomenon is rare.
4) XRD mineral analysis shows that the total clay content is less than 50%, the content of Kaolinite is obviously higher than that of Clinochlore, and the content of Illite/Smectite mixed layer is less than 30%.

These markers may provide useful evidence for identifying minor-surface-ruptures and make up for the limitations of traditional geological methods.

CONCLUSION

This study investigated the microstructures and mineral composition of the fault gouge exposed in outcrop and from boreholes in the DSF in the southern segment of the LFZ. The microstructural results revealed a series of localized brittle deformations mainly produced by stick-slip of the fault, such as fracture cleavages, straight cracks, and striations, and strongly deformed zones consisted of these deformation styles. In addition, fluid migration pores or fissures and micro- to nanometer-sized grains, related to earthquake occurrence and possibly involved by pressure solution and thermal decomposition, respectively, were also observed. The mineralogical composition revealed by the XRD analysis shows total clay content of 44% in the fault gouge from the Dachuan borehole site and 36% from the Xiaohe outcrop site. Abundant illite content, considering the result of fault slip when an earthquake occurs, was found, with 39% and 50% at Dachuan and Xiaohe sites, respectively. In conclusion, the microanalysis results of the fault gouge show that the DSF has the behavior of stick-slip, which supported by paleo-seismic researches along the fault.

A comparison analysis demonstrated that the DSF, one minor-surface-rupture fault in the southern segment of the LFZ, has

significantly different fault gouge microstructure and mineralogical composition from those in BYF with intense activity in the middle–northern segments of the LFZ. We summarized several representative characteristics of DSF that are different from BYF: 1) Macroscopically, fault gouge thickness of a single fault event is thinner. 2) Microscopically, micro-cracks in surrounding rocks and the debris reprocessing phenomenon in the gouge were rare, and discontinuous micro-cracks and untypical S-C fabrics in the gouge are common. 3) In terms of mineral composition, the total clay content is less than 50%, the content of kaolinite is obviously higher than that of clinochlore, and the content of illite/smectite mixed layer is less than 30% in the gouge. These features are systematic; therefore, comparing these fault gouge markers can help us to identify minor-surface faults.

DATA AVAILABILITY STATEMENT

The original contributions presented in the study are included in the article/Supplementary Material, further inquiries can be directed to the corresponding author.

AUTHOR CONTRIBUTIONS

YL mainly participated in the field investigation, sample collection, and analysis, and completed the writing of the article. LC mainly participated in the fieldwork, formed the idea of the article, and supported the completion of the article. YR helped with the writing of this article. YC participated in the microstructural observations of the fault gouge under a microscope. All authors contributed to the article and approved the submitted version.

FUNDING

This work was supported financially by the Second Tibetan Plateau Scientific Expedition and Research Program (STEP) (2019QZKK0901); Basic Scientific Work of the Institute of Geology, China Earthquake Administration (IGCEA1418); and National Key R&D Program of China (2019YFC0604901). The topography data used in this study (SRTM data V4) were obtained from the following website: http://srtm.csi.cgiar.org.

REFERENCES

Bos, B., Peach, C. J., and Spiers, C. J. (2000). Frictional-viscous Flow of Simulated Fault Gouge Caused by the Combined Effects of Phyllosilicates and Pressure Solution. *Tectonophysics* 327 (3), 173–194. doi:10.1016/s0040-1951(00)00168-2

Chen, J., Yang, X., Ma, S., Yang, T., and Niemeijer, A. (2016). Hydraulic Properties of Samples Retrieved from the Wenchuan Earthquake Fault Scientific Drilling Project Hole-1 (WFSD-1) and the Surface Rupture Zone: Implications for Coseismic Slip Weakening and Fault Healing. *Geochem. Geophys. Geosyst.* 17 (7), 2717–2744. doi:10.1002/2016gc006376

Chen, L., Ran, Y., Wang, H., Li, Y., and Ma, X. (2013a). Technology and Several Cases for Inter-mediate- and Long-Term Prediction of the Magnitude 6~7 Earthquake. *Seismolog Geol.* 35 (3), 480–489.

Chen, L., Ran, Y., Wang, H., Li, Y., and Ma, X. (2013b). The Lushan M_S7.0 Earthquake and Activity of the Southern Segment of the Longmenshan Fault Zone. *Chin. Sci. Bull.* 58 (28-29), 3475–3482. doi:10.1007/s11434-013-6009-6

Chen, L., Wang, H., Ran, Y., Lei, S., Li, X., Wu, F., et al. (2014). The 2013 Lushan Ms 7.0 Earthquake: Varied Seismogenic Structure from the 2008 Wenchuan Earthquake. *Seismol Res. Lett.* 85 (1), 34–39. doi:10.1785/0220130109

Chen, W. D., Tanaka, H., Huang, H. J., Lu, C. B., Lee, C. Y., and Wang, C. Y. (2007). Fluid Infiltration Associated with Seismic Faulting: Examining Chemical and Mineralogical Compositions of Fault Rocks from the Active Chelungpu Fault. *Tectonophysics* 443 (3), 243–254. doi:10.1016/j.tecto.2007.01.025

Densmore, A. L., Ellis, M. A., Li, Y., Zhou, R., Hancock, G. S., and Richardson, N. (2007). Active Tectonics of the Beichuan and Pengguan Faults at the Eastern Margin of the Tibetan Plateau. *Tectonics* 26, TC4005. doi:10.1029/2006tc001987

Dong, S.-p., Han, Z.-j., and An, Y.-f. (2017). Paleoseismological Events in the "Seismic gap" between the 2008 Wenchuan and the 2013 Lushan Earthquakes and Implications for Future Seismic Potential. *J. Asian Earth Sci.* 135, 1–15. doi:10.1016/j.jseaes.2016.12.016

Duan, Q., Yang, X., Ma, S., Chen, J., and Chen, J. (2016). Fluid-rock Interactions in Seismic Faults: Implications from the Structures and Mineralogical and Geochemical Compositions of Drilling Cores from the Rupture of the 2008 Wenchuan Earthquake, China. *Tectonophysics* 666, 260–280. doi:10.1016/j.tecto.2015.11.008

Fu, B., Wang, P., Kong, P., Zheng, G., Wang, G., and Shi, P. (2008). Preliminary Study of Coseismic Fault Gouge Occurring in the Slip Zone of the Wenchuan Ms 8.0 Earthquake and its Tectonic Implication. *Acta Petrol. Sin* 24 (10), 2237–2243.

Gao, M., Zeilinger, G., Xu, X., Tan, X., Wang, Q., and Hao, M. (2016). Active Tectonics Evaluation from Geomorphic Indices for the central and the Southern Longmenshan Range on the Eastern Tibetan Plateau, China. *Tectonics* 35 (8), 1812–1826. doi:10.1002/2015TC004080

Han, L., Zhou, Y., Chen, J., Ma, S., Yang, X., He, C., et al. (2010). Structural Characters of Co-seismic Fault Gouge in Bed Rocks during the Wenchuan Earthquake. *Quat. Sci.* 30 (4), 745–758.

Han, R., Shimamoto, T., Hirose, T., Ree, J.-H., and Ando, J.-i. (2007). Ultralow Friction of Carbonate Faults Caused by Thermal Decomposition. *Science* 316 (5826), 878–881. doi:10.1126/science.1139763

He, C., Wang, Z., and Yao, W. (2007). Frictional Sliding of Gabbro Gouge under Hydrothermal Conditions. *Tectonophysics* 445 (3), 353–362. doi:10.1016/j.tecto.2007.09.008

He, C., Yao, W., Wang, Z., and Zhou, Y. (2006). Strength and Stability of Frictional Sliding of Gabbro Gouge at Elevated Temperatures. *Tectonophysics* 427 (1), 217–229. doi:10.1016/j.tecto.2006.05.023

Isaacs, A. J., Evans, J. P., Song, S.-R., and Kolesar, P. T. (2007). Structural, Mineralogical, and Geochemical Characterization of the Chelungpu Thrust Fault, Taiwan. *Terr. Atmos. Ocean. Sci.* 18 (2), 183–221. doi:10.3319/tao.2007.18.2.183(tcdp)

Lei, S., Ran, Y., Wang, H., Chen, L., Li, X., Wu, F., et al. (2014). Discussion on whether There Are Coseismic Surface Ruptures of the Lushan M_S7.0 Earthquake at Longmen Area and its Implicaitons. *Seismolog Geol.* 36 (1), 266–274. doi:10.3969/j.issn.0253-4967.2014.01.022

Li, C., Xu, X., Gan, W., Wen, X., Zheng, W., Wei, Z., et al. (2013a). Seismogenic Structures Associated with the 20 April 2013 M_S7.0 Lushan Earthquake, Sichuan Province. *Seismolog Geol.* 35 (3), 671–683.

Li, H., Wang, H., Xu, Z., Si, J., Pei, J., Li, T., et al. (2013b). Characteristics of the Fault-Related Rocks, Fault Zones and the Principal Slip Zone in the Wenchuan Earthquake Fault Scientific Drilling Project Hole-1 (WFSD-1). *Tectonophysics* 584, 23–42. doi:10.1016/j.tecto.2012.08.021

Liu, D., Li, H., Lee, T.-Q., Sun, Z., Liu, J., Han, L., et al. (2016). Magnetic mineral Characterization Close to the Yingxiu-Beichuan Fault Surface Rupture Zone of the Wenchuan Earthquake (Mw 7.9, 2008) and its Implication for Earthquake Slip Processes. *J. Asian Earth Sci.* 115, 468–479. doi:10.1016/j.jseaes.2015.10.019

Moore, D. E., Summers, R., and Byerlee, J. D. (1989). Sliding Behavior and Deformation Textures of Heated Illite Gouge. *J. Struct. Geol.* 11 (3), 329–342.

Ran, Y.-K., Chen, W.-S., Xu, X.-W., Chen, L.-C., Wang, H., Yang, C.-C., et al. (2013). Paleoseismic Events and Recurrence Interval along the Beichuan-Yingxiu Fault of Longmenshan Fault Zone, Yingxiu, Sichuan, China. *Tectonophysics* 584 (0), 81–90. doi:10.1016/j.tecto.2012.07.013

Ran, Y., Chen, L., Chen, J., Wang, H., Chen, G., Yin, J., et al. (2010a). Paleoseismic Evidence and Repeat Time of Large Earthquakes at Three Sites along the Longmenshan Fault Zone. *Tectonophysics* 491 (1), 141–153. doi:10.1016/j.tecto.2010.01.009

Ran, Y., Chen, W., Xu, X., Chen, L., Wang, H., and Li, Y. (2014). Late Quaternary Paleoseismic Behavior and Rupture Segmentation of the Yingxiu-Beichuan Fault along the Longmen Shan Fault Zone, China. *Tectonics* 33 (11), 2218–2232. doi:10.1002/2014tc003649

Ran, Y., Shi, X., Wang, H., Chen, L., Chen, J., Liu, R., et al. (2010b). The Maximum Coseismic Vertical Surface Displacement and Surface Deformation Pattern Accompanying the Ms 8.0 Wenchuan Earthquake. *Chin. Sci. Bull.* 55 (9), 841–850. doi:10.1007/s11434-009-0453-3

Reinen, L. A. (2000). Seismic and Aseismic Slip Indicators in Serpentinite Gouge. *Geology* 28 (2), 135–138. doi:10.1130/0091-7613(2000)028<0135:saasii>2.3.co;2

Si, J., Li, H., Kuo, L., Pei, J., Song, S., and Wang, H. (2014). Clay mineral Anomalies in the Yingxiu-Beichuan Fault Zone from the WFSD-1 Drilling Core and its Implication for the Faulting Mechanism during the 2008 Wenchuan Earthquake (Mw 7.9). *Tectonophysics* 619-620, 171–178. doi:10.1016/j.tecto.2013.09.022

Tanaka, H., Fujimoto, K., Ohtani, T., and Ito, H. (2001). Structural and Chemical Characterization of Shear Zones in the Freshly Activated Nojima Fault, Awaji Island, Southwest Japan. *J. Geophys. Res.* 106 (B5), 8789–8810. doi:10.1029/2000jb900444

Wang, H., Li, H., Si, J., Sun, Z., and Huang, Y. (2014). Internal Structure of the Wenchuan Earthquake Fault Zone, Revealed by Surface Outcrop and WFSD-1 Drilling Core Investigation. *Tectonophysics* 619-620, 101–114. doi:10.1016/j.tecto.2013.08.029

Wang, M., Jia, D., Lin, A., Shen, L., Rao, G., and Li, Y. (2013). Late Holocene Activity and Historical Earthquakes of the Qiongxi Thrust Fault System in the Southern Longmen Shan Fold-And-Thrust belt, Eastern Tibetan Plateau. *Tectonophysics* 584 (1), 102–113. doi:10.1016/j.tecto.2012.08.019

Xu, X., Chen, G., Yu, G., Cheng, J., Tan, X., Zhu, A., et al. (2013a). Seismogenic Structure of Lushan Earthquake and its Relationship with Wenchuan Earthquake. *Earth Sci. Front.* 20 (3), 11–20. doi:10.1130/G25462A.1

Xu, X., Wen, X., Han, Z., Chen, G., Li, C., Zheng, W., et al. (2013b). Lushan M_S7.0 Earthquake: A Blind reserve-fault Event. *Chin. Sci. Bull.* 58 (Z2), 3437–3443. doi:10.1007/s11434-013-5999-4

Xu, X., Wen, X., Yu, G., Chen, G., Klinger, Y., Hubbard, J., et al. (2009). Coseismic Reverse- and Oblique-Slip Surface Faulting Generated by the 2008 Mw 7.9 Wenchuan Earthquake, China. *Geology* 37 (6), 515–518. doi:10.1130/g25462a.1

Yang, X., Jiang, P., Song, F., Liang, X., Chen, X., and Deng, Z. (1999). The Evidence of the South Longmenshan Fault Zones Cutting Late Quaternary Stratum. *Seismolog Geol.* 21 (4), 341–345. doi:10.3969/j.issn.0253-4967.1999.04.007

Yuan, R., Zhang, B., Xu, X., and Lin, C. (2013). Microstructural Features and Mineralogy of clay-rick Fault Gouge at the Northern Segment of the Yingxiu-Beichuan Fault, China. *Seismolog Geol.* 35 (4), 685–700. doi:10.3969/j.issn.0253-4967.2013.04.001

Yuan, R., Zhang, B., Xu, X., Lin, C., Si, L., and Li, X. (2014). Features and Genesis of Micro-nanometer-sized Grains on Shear Slip Surface of the 2008 Wenchuan Earthquake. *Sci. China Earth Sci.* 57 (8), 1961–1971. doi:10.1007/s11430-014-4859-7

Zhang, B., Lin, C., and Shi, L. (2002). Microstructural Features of Fault Gouges from Tianjing-Shan-Xiangshan Fault Zone and Their Geological Implications. *Sci. China Ser. D-earth Sci.* 45 (1), 72–80. doi:10.1007/bf02879698

Zhang, P., Xu, X., Wen, X., and Ran, Y. (2008). Slip Rates and Recurrence Intervals of the Longmen Shan Active Fault Zone, and Tectonic Implications for the Mechanism of the May 12 Wenchuan Earthquake, 2008, Sichuan, China. *Chin. J. Geophys.* 51 (4), 1066–1073. doi:10.3321/j.issn:0001-5733.2008.04.015

Conflict of Interest: The authors declare that the research was conducted in the absence of any commercial or financial relationships that could be construed as a potential conflict of interest.